


Complete electrodynamics of a BCS superconductor with μeV energy scales: Microwave spectroscopy on titanium at mK temperatures

Markus Thiemann, Martin Dressel, and Marc Scheffler

1. Physikalisches Institut, Universität Stuttgart, Pfaffenwaldring 57, D-70569 Stuttgart, Germany

 (Received 8 March 2018; revised manuscript received 23 April 2018; published 20 June 2018)

We performed resonant microwave measurements on superconducting titanium (Ti) down to temperatures of 40 mK, well below its critical temperature $T_c \approx 0.5$ K. Our wide frequency range 3.3–40 GHz contains the zero-temperature energy gap $2\Delta_0$ and allows us to probe the full electrodynamics of the superconducting state, including excitations across the gap and the low-frequency responses of superfluid condensate and thermal quasiparticles. The observed behavior follows the predictions of the BCS-based Mattis-Bardeen formalism, which implies that superconducting Ti is in the dirty limit, in agreement with our determination of the scattering rate. We directly determine the temperature dependence of the energy gap, which is in accordance with BCS predictions, and $2\Delta_0/k_B T_c \approx 3.5$ with $\Delta_0 \approx 72 \mu\text{eV}$. We also evaluate the penetration depth, and we characterize the behavior of superconducting Ti in external magnetic field.

DOI: [10.1103/PhysRevB.97.214516](https://doi.org/10.1103/PhysRevB.97.214516)

I. INTRODUCTION

Optical spectroscopy is a versatile tool to investigate the fundamental electronic characteristics of superconductors [1,2]: single-particle excitations indicate the superconducting energy gap; the superfluid condensate and the penetration depth are probed via the out-of phase response; and the quasiparticle dynamics are sensed via subgap absorption. These experimental virtues have led to such groundbreaking results as the first observations of the superconducting energy gap 2Δ via far-infrared spectroscopy and of the condensate reactance via microwave studies of Pb and Sn [3–5] around the time that BCS theory was developed [6]. Microwave measurements also gave the first robust evidence in the 1990s for the linear temperature dependence of the penetration depth in cuprate superconductors, which suggests *d*-wave symmetry of the superconducting order parameter [7–9]. Consequently, numerous superconducting materials have been studied with electrodynamic experiments in the infrared, THz, or microwave spectral range [1,10–12]. Most of these experiments were performed at temperatures of liquid ^4He , whereas only very few optical studies addressed temperatures below 1 K [13–18]. Experimental challenges for a long time precluded electrodynamic studies of superconductors at ultralow temperatures [19], and thus all superconductors with critical temperature T_c well below 1 K could not be probed by optics, with microwave spectroscopy being particularly relevant (thermal energy $k_B T$ for 1 K corresponds to $86 \mu\text{eV}$ photon energy $\hbar\omega$ or 21 GHz). Considering the wide range of unconventional low- T_c superconductors that are presently studied at mK temperatures with other techniques, spanning heavy-fermion superconductors [20], materials near a superconductor-insulator transition [21,22], ultralow density superconductors [23], or the $\text{LaAlO}_3/\text{SrTiO}_3$ interface [24], the lack of optical data is quite unfortunate.

Recent experimental advances now allow microwave spectroscopy experiments in $^3\text{He}/^4\text{He}$ dilution refrigerators [19,25–30], and thus the microwave response at mK

temperatures of such superconducting materials with rather low T_c comes into focus. These experiments operate in a previously unexplored regime, considering that the accessible GHz spectral range includes frequencies both smaller and larger than 2Δ of mK superconductors [19] and that T_c or 2Δ can be much smaller than other energy scales, e.g., the scattering rate. While this newly accessible experimental regime prompts studies on numerous exotic superconducting states, at the same time it calls for investigations of superconductors with T_c well below 1 K that are considered conventional superconductors and thus allow investigations of BCS-like behavior in previously inaccessible parameter ranges and that at the same time can act as references for similar experiments on unconventional low- T_c superconductors. This is our motivation to choose the elemental superconductor Ti with T_c around 0.5 K [31–35] for this investigation of the complete electrodynamics of a mK superconductor. The role of sample purity for superconductivity in Ti is evident from early experiments [36,37] as well as more detailed recent work [34,35]. Furthermore, de Haas-van Alphen measurements on Ti indicate different Fermi sheets with effective masses ranging from $m^* = 1m_e$ to $m^* = 3m_e$ [38,39], making titanium a candidate for multiband superconductivity, like recently observed for another elemental superconductor, Pb [40]. Superconductivity in Ti is also exploited in various mK devices [41–43].

We employ a microwave multimode resonator to obtain the optical conductivity of superconducting Ti for frequencies and temperatures ranging from 3–40 GHz and 40–600 mK, respectively, smoothly crossing from $\hbar\omega \ll k_B T$ to $\hbar\omega \gg k_B T$. This allows us to measure across the superconducting energy gap and observe the temperature dependence of the gap as a unique feature in our optical conductivity spectra. Furthermore, we evaluate the full electrodynamic response of Ti within the BCS framework, and we investigate the superconducting state of Ti in an external magnetic field.

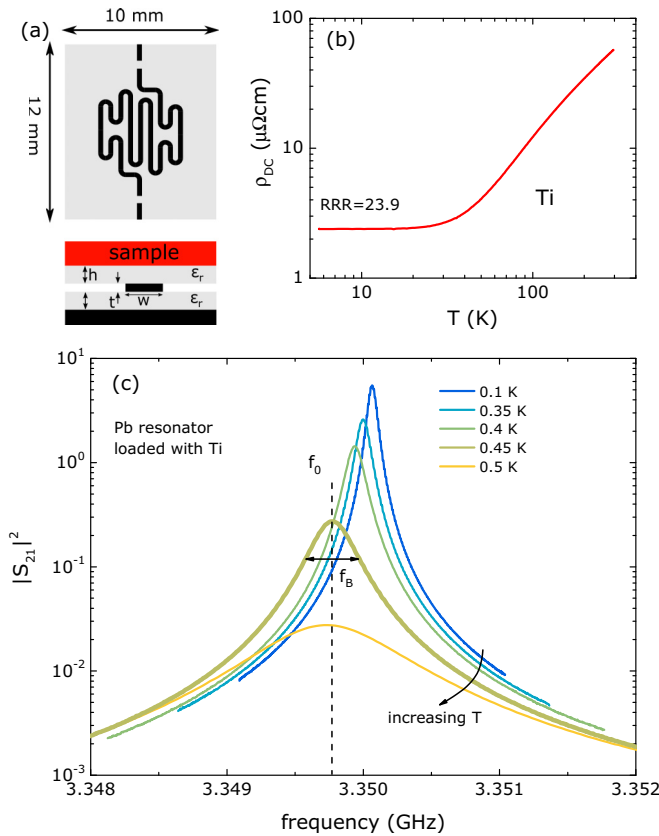


FIG. 1. (a) Schematic of a stripline resonator. (Top) Top view on the center conductor. (Bottom) Cross section with relevant parameters: dielectric constant ϵ_r and thickness h of the dielectric, center conductor thickness t and width w . (b) Temperature dependence of the dc resistivity of Ti sample with residual resistance ratio [RRR = $\rho_{dc}(300\text{ K})/\rho_{dc}(5.6\text{ K})$] of 23.9. (c) Temperature evolution of the lowest measured resonance at $f_0 = 3.35$ GHz: transmission coefficient S_{21} measured with a vector network analyzer and an additional room-temperature amplifier. Note the shift of the resonant bandwidth f_B (full width at half maximum) and resonance frequency f_0 due to the temperature-dependent surface impedance of the sample.

II. EXPERIMENT

To combine microwave spectroscopy with mK temperatures, we employ superconducting stripline resonators [45–48]. A stripline is formed by a planar center conductor, sandwiched between two dielectrics followed by two ground planes, as shown in the schematic drawing of Fig. 1(a). The center conductor has a meandered shape to increase its length beneath the sample. This allows us to achieve fundamental frequencies of about 1.5 GHz [48]. The gaps in the center conductor define a one-dimensional resonant structure, with harmonics spaced equally in frequency. By measuring several of the harmonics, we gain information about the frequency dependence. In the used stripline geometry the sample acts as ground plane, and therefore a change in the microwave properties (i.e., the optical conductivity at GHz frequencies) of the sample acts as a perturbation on the resonator. This results in a shift of the resonance frequency f_0 and a change in the resonant bandwidth f_B compared to the unperturbed ideal resonator. f_B and f_0 are connected to the quality factor

Q , which is commonly used to characterize resonators, via $Q = f_0/f_B$. The measured quantities f_B and f_0 , as defined in Fig. 1(c), can be related to the surface impedance $Z_s = R_s - iX_s$ of the sample via cavity perturbation theory [49]:

$$R_s - i\Delta X_s = G \left(\frac{f_B^{\text{sample}}}{2} - i\Delta f_0 \right). \quad (1)$$

Here Δf_0 is the change in the resonance frequency that is caused by the sample compared to an unperturbed resonator. G is the resonator constant, which depends on the resonator geometry and the interaction of the electromagnetic fields with the sample. To determine $\Delta f_0(T)$ from the experimentally measured frequencies $f_0(T)$, we have to know the absolute value of Δf_0 for one reference temperature, and to this end we assume that R_s and X_s match at temperatures above T_c , in the metallic state, and we introduce the appropriate additive constant to the X_s data. This procedure is valid for frequencies below the scattering rate of the sample, i.e., in the Hagen-Rubens regime [50]. Assuming local electrodynamics, where the mean free path of the electrons is shorter than the skin depth, we can then calculate the optical conductivity $\sigma = \sigma_1 + i\sigma_2$ via [50]:

$$\sigma = \frac{i\omega\mu_0}{Z_s^2}. \quad (2)$$

The dimensions of the stripline [see schematic cross section in Fig. 1(a)] are as follows to match the characteristic impedance of $50\ \Omega$ of the external microwave circuitry [51]: thickness $h = 127\ \mu\text{m}$ and dielectric constant $\epsilon_r \approx 10$ of the dielectric, width $w = 50\ \mu\text{m}$ and thickness $t = 1\ \mu\text{m}$ of the center conductor. The gaps in the inner conductor, which define the length of the resonator, were $100\ \mu\text{m}$ wide to provide appropriate coupling.

To be as sensitive as possible to the sample of interest, the internal losses of the resonator have to be minimized. Therefore we use sapphire as a dielectric due to its low microwave losses [52]. The conductive parts of the resonator, colored black in Fig 1(a), are made of superconducting Pb with a $T_c \approx 7.2\text{ K}$. The center conductor is formed by thermal evaporation using a shadow mask. With pure Pb resonators, where the sample is Pb as well, quality factors exceeding 10^5 can be achieved [53]. The resonator is mounted in a brass box, which is directly connected to the cold finger of a commercial dilution refrigerator.

The Ti sample (dimensions: $9.5 \times 9.5 \times 1\ \text{mm}^3$) was cut from a Ti plate with purity of 99.999% [54]. Figure 1(b) shows the temperature dependence of the dc resistivity ρ_{dc} of a separate sample with dimensions of $10 \times 1 \times 1\ \text{mm}^3$ cut from the same Ti plate, measured in four-point geometry in a ^4He cryostat. The comparably low residual resistance ratio (RRR) value of 23.9 and the flattening of ρ_{dc} at around 30 K indicate substantial defect scattering present in the polycrystalline sample. Using the plasma frequency given in Ref. [55] $\omega_p = 20300\ \text{cm}^{-1}$ and $\Gamma_\rho = \epsilon_0\omega_p^2\rho_{dc}$, we can estimate the scattering rate to $\Gamma_\rho/2\pi = 490\ \text{GHz}$. This value is well above our measurement frequencies and thus justifies the assumption of our sample being in the Hagen-Rubens regime.

We performed mK microwave measurements on the same sample twice, and we could easily determine T_c from a sharp drop in the resonant bandwidth $f_B(T)$ at the lowest frequency.

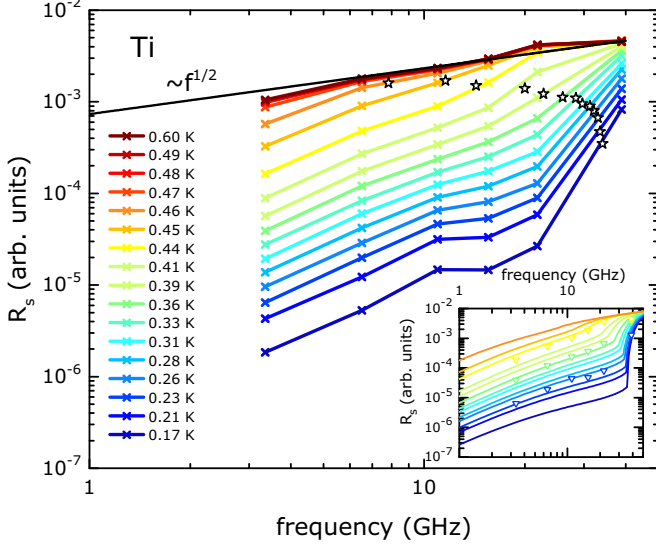


FIG. 2. Frequency dependence of the surface resistance of Ti for temperatures across T_c . The black line is a square root fit to the lowest five frequencies for $T = 0.60$ K, well above T_c . In the superconducting state a change in the frequency dependence is visible when crossing the energy gap 2Δ . The open stars denote the frequency of the theoretically expected energy gap $2\Delta(T)$ at each temperature. (Inset) Calculated surface resistance using the Mattis-Bardeen formalism with a $T_c = 0.47$ K and $2\Delta_0/k_B T_c = 3.53$. The open triangles are data from the main panel for temperatures $T = 0.23$ K, 0.36 K, and 0.44 K.

In the first measurement, we observed $T_c \approx 0.47$ K. Then the sample was polished, and in the second measurement we found $T_c \approx 0.49$ K.

III. DATA ANALYSIS

Superconducting Pb resonators bear loss mechanisms that originate from the polycrystalline structure of the evaporated Pb, defects and oxides on the conducting surfaces, and coupling losses [56,57]. In our temperature range $T < 1$ K, these effects may depend on frequency, but are usually temperature independent. Due to Eq. (1) the residual losses can be expressed in terms of a bandwidth f_B^{res} adding to the bandwidth f_B^{sample} caused by the intrinsic losses of the sample. The measured bandwidth can then be expressed by $f_B(T) = f_B^{\text{sample}}(T) + f_B^{\text{res}}$ allowing us to determine $f_B^{\text{res}} = f_B(T_0)$, where T_0 denotes the lowest measured temperature. At low temperatures, the losses of a superconductor become very small and $f_B^{\text{sample}}(T) \ll f_B^{\text{res}}$. $f_B^{\text{sample}}(T)$ can then be calculated via $f_B^{\text{sample}}(T) = f_B(T) - f_B(T_0) = f_B(T) - f_B^{\text{res}}$. This procedure is certainly valid for fully gapped superconductors with a T_c that is a few times higher than the lowest measurable temperature and frequencies below the energy gap $2\Delta_0 = 2\Delta(T = 0)$. The surface impedance is then determined from f_B^{sample} via Eq. (1).

In Fig. 2 the surface resistance $R_s(\omega)$ for different temperatures in the superconducting as well as in the metallic state are shown. For the first five frequencies, we applied the above correction procedure. However, for the highest frequency we

cannot expect that the condition $f_B^{\text{sample}}(T) \ll f_B^{\text{res}}$ is fulfilled, since the frequency is near the expected energy gap $2\Delta_0/h = 3.53k_B T_c/h = 34$ GHz of Ti, and absorption by breaking Cooper pairs is possible even at the lowest temperature. Therefore, we introduce a different approach to correct f_B at this frequency above the energy gap, in particular we consider the metallic state above T_c as reference. As mentioned above, with the normal-state scattering rate much larger than our probing frequencies we are in the Hagen-Rubens regime of metals [50]. This means that here σ_1 is basically frequency independent and $\sigma_1 \gg \sigma_2$. Following Eq. (2), $R_s = X_s \propto \sqrt{\omega}$ is expected for the surface impedance above T_c . We now fit a square-root frequency dependence to R_s at 0.6 K for our first five frequencies (3.35–21.79 GHz), which lie below the energy gap $2\Delta_0$ where the correction method discussed above applies. This fit, shown as black line in Fig. 2, we extrapolate to obtain the expected R_s value for 38.91 GHz. We now use this value to analyze the experimental, temperature-dependent R_s data at this frequency by introducing the appropriate value of f_B^{res} that matches the experimental R_s at 0.6 K to this expected value. The inset of Fig. 2 shows the expected frequency dependence of R_s of Ti, calculated within the Mattis-Bardeen formalism [44] and assuming an energy gap $2\Delta_0 = 3.53k_B T_c \hat{=} 34$ GHz. Clearly, the phenomenology of frequency- and temperature-dependent R_s observed in our data match these theoretical expectations. In particular, the sharp rise in $R_s(\omega)$ around 40 GHz for lowest temperature and moving to lower frequencies with increasing temperature marks the energy gap $2\Delta/h$. In Fig. 2 the frequency that corresponds to $2\Delta(T)$ is indicated by the black-edged stars for the different temperatures.

IV. RESULTS AND DISCUSSION

A. Electrodynamics of the superconducting state

The interpretation of optical spectra measured on superconductors is usually done with respect to the complex optical conductivity $\sigma = \sigma_1 + i\sigma_2$, where σ_1 is connected to the absorption rate and σ_2 to the phase shift of the electromagnetic wave. For dirty superconductors, with scattering rate Γ much larger than the superconducting energy gap $2\Delta/\hbar$, the optical conductivity is treated within the Mattis-Bardeen theory [44]. The theoretically expected frequency and temperature dependences are shown as solid lines in Figs. 4(a), 4(b) and Figs. 4(e), 4(f) respectively. In the superconducting state the energy gap forms around the Fermi surface, and the states within the energy gap are transferred to the edge of the energy gap, forming square-root singularities. A depiction of the density of states in a fully gapped superconductor is shown in Fig. 3. For frequencies below the energy gap, only the thermally excited quasiparticles can absorb energy and contribute to σ_1 . This contribution to σ_1 we denote as σ_1^{th} and is shown as blue arrows in Fig. 3. At very low frequencies, the temperature dependence $\sigma_1(T)$ exhibits a so-called coherence peak, a broad maximum at temperatures slightly below T_c , which occurs due to the singularities in the density of states and the coherence factors [67]. In Fig. 4(e), such a coherence peak in $\sigma_1(T)$ is a pronounced feature at the lowest calculated frequency. If the frequency is greater than $2\Delta(T)$, quasiparticles can be excited

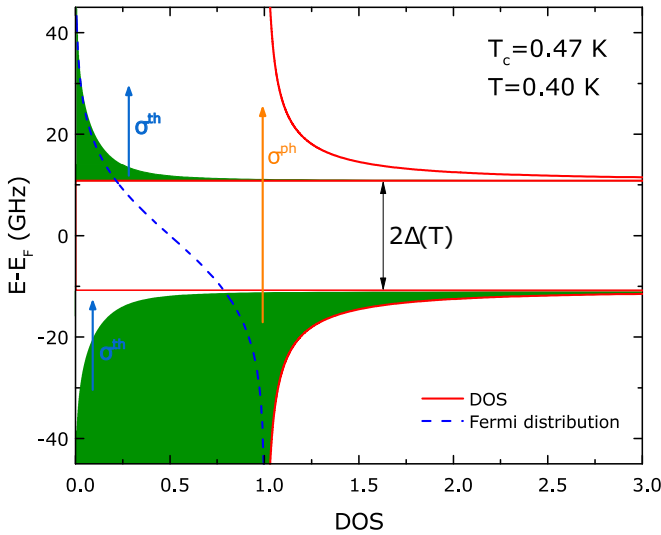


FIG. 3. Calculated density of states of an s -wave superconductor with a $T_c = 0.47$ K at $T = 0.4$ K. Green areas indicate occupied states. The blue dashed line represents the Fermi distribution at $T = 0.4$ K. The blue and orange arrows indicate the possible transitions contributing to σ^{th} and σ^{ph} , respectively.

across the energy gap, leading to an extra absorption channel σ_1^{ph} shown as orange arrow in Fig. 3. The total conductivity $\sigma_1 = \sigma_1^{\text{th}} + \sigma_1^{\text{ph}}$ then exhibits upturns as a function of ω or T when the excitation frequency matches the energy gap $2\Delta(T)$,

i.e., the energy gap can be observed as a sharp kink in the $\sigma_1(\omega, T)$ manifold.

Figures 4(a) and 4(b) show the frequency dependence of σ_1 and σ_2 , respectively, for temperatures above and below T_c . Here the conductivity at each frequency was normalized to the normal-state conductivity σ_n measured above T_c . When entering the superconducting state $T < T_c = 0.47$ K, we observe a reduction of $\sigma_1(\omega)$ for the highest five frequencies, whereas for the lowest, at $f_0 = 3.35$ GHz, σ_1 increases first when lowering the temperature below T_c . This is due to the energy gap opening, and spectral weight of $\sigma_1(\omega)$ is shifted to lower frequencies, resulting in a reduced $\sigma_1(\omega)$ around the energy gap. In Fig. 4(b) the frequency dependence of σ_2 for various temperatures is shown. σ_1 and σ_2 are connected by the Kramers-Kronig relations. At very low temperatures and at frequencies below the energy gap, the overall behavior of σ_1 is dominated by the $\delta(\omega)$ peak at zero frequency caused by the superfluid condensate whereas quasiparticle contributions to σ_1 vanish. As the Kramers-Kronig transformation of the δ peak, a $1/f$ frequency dependence is expected for $\sigma_2(\omega)$ in the superconducting state, which is indicated by the dashed line in Fig. 4(b) and experimentally observed for frequencies below the gap.

Figures 4(c), 4(d) show the temperature dependence of the optical conductivity at different frequencies. At the lowest shown frequency, $\sigma_1(T)$ exhibits a pronounced upturn just below T_c as the sample enters the superconducting state. This is the before-mentioned coherence peak. Although BCS theory and the Mattis-Bardeen formalism were developed in

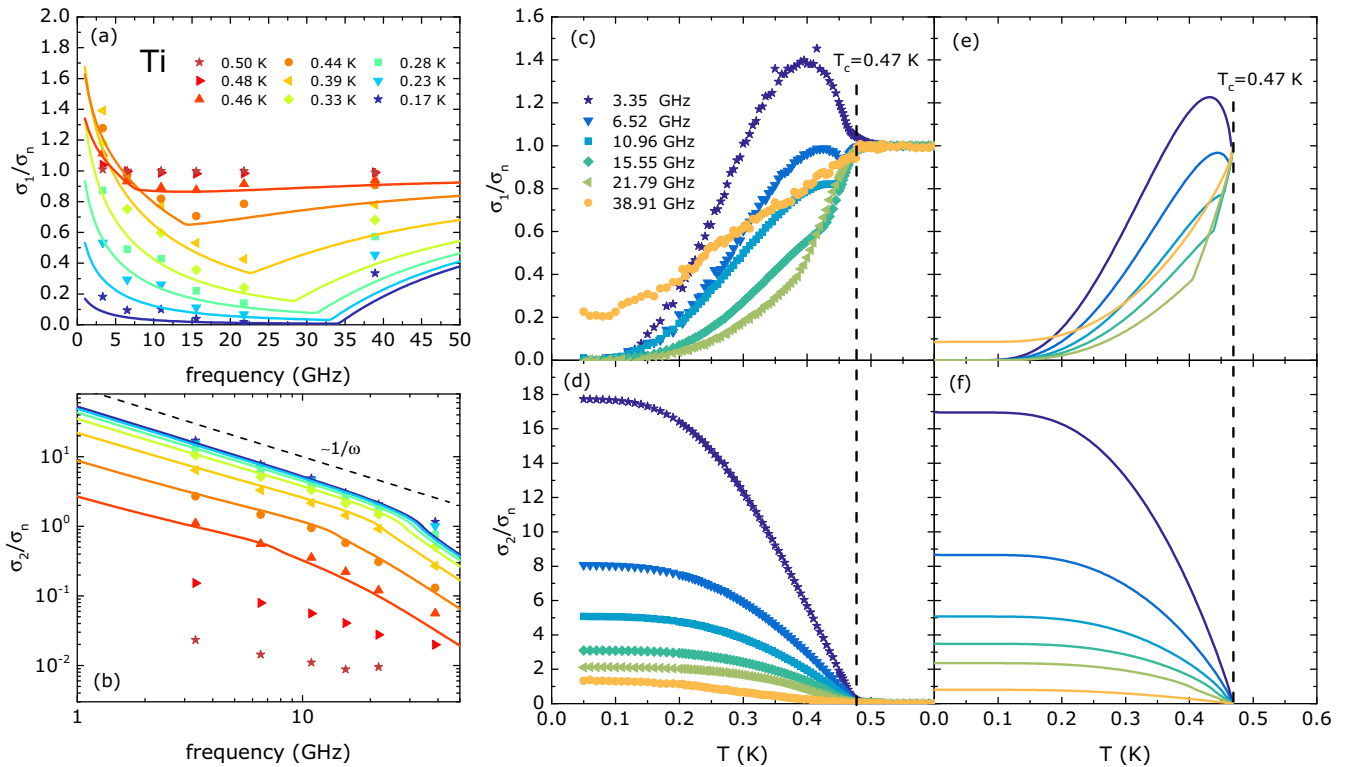


FIG. 4. (a), (b) Frequency dependence of $\sigma = \sigma_1 + i\sigma_2$ at various temperatures. The solid lines represent the frequency behavior calculated from the Mattis-Bardeen equations using a $T_c = 0.47$ K and $2\Delta_0/k_B T_c = 3.53$. The energy gap appears in $\sigma_1(\omega)$ as a kink. (c), (d) Temperature dependence of σ at different measured frequencies. (e), (f) Calculated optical conductivity using the Mattis-Bardeen formalism with $T_c = 0.47$ K and $2\Delta_0/k_B T_c = 3.53$.

the late 1950s, the coherence peak in the optical conductivity was observed only in the 1990s and remains in the focus of microwave experiments on superconductors [58–62]. As we go up in frequency, $\sigma_1(T)$ in the superconducting state decreases compared to lower frequencies due to the reduced number of states the thermal quasiparticles can be excited into. At the highest measured frequency of 38.91 GHz, $\sigma_1(T)$ does not vanish at low temperatures, since the excitation frequency is above the zero-temperature energy gap $2\Delta_0$, and therefore breaking of quasiparticles is possible even for lowest temperatures.

Figure 4(d) shows the imaginary part $\sigma_2(T)$ of the optical conductivity, which is mainly related to the superfluid in the superconducting state at low frequencies. At low temperatures $\sigma_2(T)$ becomes constant, because then all quasiparticles are condensed into the superfluid. The qualitative behavior of $\sigma(T)$ fits quite well with the behavior predicted by Mattis-Bardeen theory, which is shown in Figs. 4(e) and 4(f) as comparison to Figs. 4(c) and 4(d).

B. Superconducting energy gap

In principle one can quantify the superconducting energy gap 2Δ from measured data by fitting the $\sigma(\omega)$ spectra to the theoretical expectation [63–65], in the simplest case based on the Mattis-Bardeen formalism [2,44,66]. The accuracy of determining the energy gap this way depends on the experimental frequency resolution, which in our case is not sufficient for meaningful fits with Δ as free parameter. We therefore follow a different approach by evaluating $\sigma_1(T)$ at a fixed frequency. Here we expect an abrupt change in the temperature dependence once the excitation frequency matches the energy gap 2Δ , as visible in Fig. 4(e). Since 2Δ is temperature dependent, different excitation energies will match the energy gap at different temperatures. The advantage of looking at $\sigma_1(T)$ is that our temperature resolution is much higher than our frequency resolution.

For the intermediate frequencies (6.52–21.79 GHz) we can easily observe this abrupt change in temperature dependence, as marked by the red arrows in the inset of Fig. 5, which reproduces data of Fig. 4(c) close to T_c . The main panel of Fig. 5 shows the values for the energy gap $2\Delta(T)$ determined by this method for both measurements. The blue solid lines are the temperature dependence of the energy gap predicted by weak coupling BCS theory with $2\Delta_0/k_B T_c \approx 3.53$. The dashed lines are fits of the BCS temperature dependence with T_c and the ratio $2\Delta_0/k_B T_c$ as free fit parameters. The values for T_c and $2\Delta_0/k_B T_c$ that we obtain from the fits are 0.464 K and 3.59 for the first measurement and 0.493 K and 3.30 for the second measurement, respectively. Ideally, one would determine Δ_0 from data at temperatures much lower than T_c while the direct determination of $2\Delta(T)$ from our microwave data only applies for frequencies lower than 22 GHz, corresponding to temperatures higher than 0.38 K. In spite of this experimental limitation, we can estimate the zero-temperature energy gap Δ_0 of Ti to be around 17 GHz $\approx 72 \mu\text{eV}$ by safely assuming that the BCS-like electrodynamic in superconducting Ti that is evident in our data will continue down to lowest temperatures.

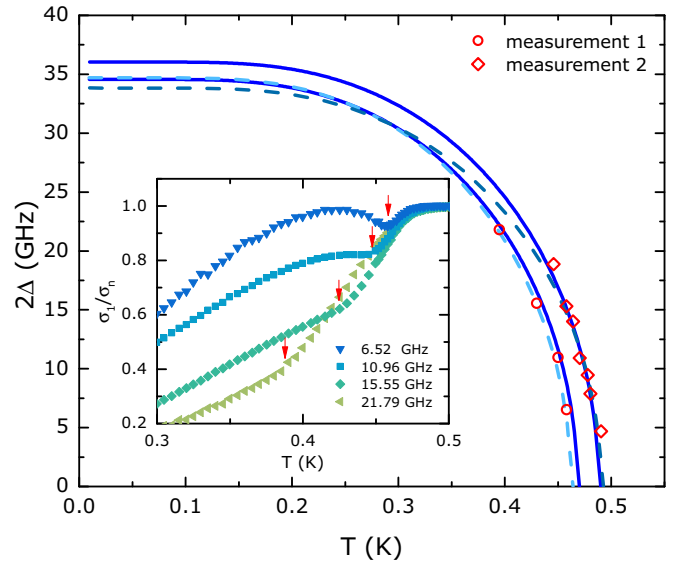


FIG. 5. (Inset) As a function of temperature σ_1 shows distinct kinks (marked by arrows) indicating the temperature where $\Delta(T)$ matches the applied microwave frequency. (Main) Circles and diamonds indicate the energy gap for the two measurements as determined by the procedure of the inset. The solid lines are BCS predictions with $2\Delta_0/k_B T_c = 3.53$. Dashed lines are fits of $2\Delta(T)$ to the data with T_c and $2\Delta_0/k_B T_c$ as fit parameters.

C. Superfluid density, penetration depth, and scattering rate

So far we have only considered the response of the thermal quasiparticles and the breaking of Cooper pairs, which contribute to σ_1 . The response of the superfluid is encoded in the out-of-phase response σ_2 . At low frequencies the superfluid density ρ_s is connected to σ_2 via [67]

$$\rho_s(T) = 1/\lambda(T)^2 = \lim_{\omega \rightarrow 0} \mu_0 \omega \sigma_2(\omega, T). \quad (3)$$

In the clean case where $\Gamma/2\pi \rightarrow 0$, the spectral weight in $\sigma_1(\omega)$ available to condense into the superfluid is the full spectral weight of the normal-state Drude peak, which is given in terms of the plasma frequency by $\rho_{s00} = \mu_0 \epsilon_0 \omega_p^2$. With increasing scattering, spectral weight is shifted to higher frequencies, out of the range where it condenses into the superfluid. Therefore an increase of scattering causes a decrease of the superfluid density. In the presence of scattering, the temperature dependence of the superfluid density can be calculated by

$$\rho_s(T) = \rho_{s00} 2\pi k_B T \sum_{\omega_n > 0}^{\infty} \frac{1}{\sqrt{\omega_n^2 + \Delta(T)^2} + \frac{\Gamma_{sf}}{2\hbar} \omega_n^2 + \Delta(T)^2}, \quad (4)$$

where $\omega_n = 2\pi k_B T(n + 1/2)$ are the Matsubara frequencies [68]. The dashed black line in Fig. 6 is a fit of Eq. (4) to the measured superfluid density obtained via Eq. (3) from our σ_2 data at 6.52 GHz, where T_c [which enters Eq. (4) via the temperature dependence of Δ , which is assumed BCS-like] and Γ_{sf} were fit parameters. From the fit we determine $T_c = 0.474$ K and $\Gamma_{sf}/2\pi = 430$ GHz. Comparing $\Gamma_{sf}/2\pi$ with the scattering rate from resistivity $\Gamma_\rho/2\pi = 490$ GHz, we find them in good agreement. The fit allows us to extract the

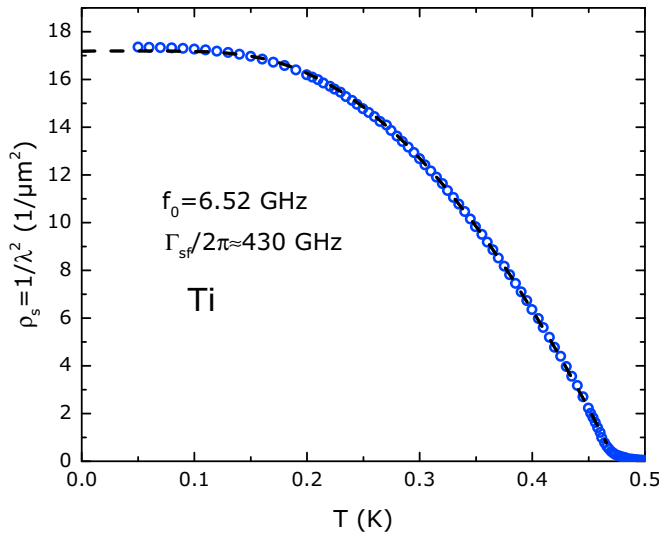


FIG. 6. Temperature dependence of the superfluid density ρ_s calculated from the σ_2 data obtained at $f_0 = 6.52$ GHz. The black dashed line is a fit for BCS-weak-coupling superfluid density in the presence of disorder, with T_c and the scattering rate $\Gamma/2\pi$ as fit parameters.

zero-temperature superfluid density $\rho_s(0\text{K})$ and consequently the zero-temperature penetration depth $\lambda_0 = 1/\sqrt{\rho_s(0\text{K})} = 241$ nm. Performing such fits to the data for the different resonances in the frequency range 3.35–15.55 GHz, we obtain an average scattering rate $\overline{\Gamma_{\text{sf}}}/2\pi = 418 \pm 43$ GHz and an average zero-temperature penetration depth $\overline{\lambda_0} = 238 \pm 9$ nm.

Next we would like to comment on the change in T_c after polishing, and the absence of multigap features in our data. (All theory descriptions above consider only a single superconducting gap, and all our data, most notably the temperature-dependent penetration depth in Fig. 6, are fully consistent with this assumption.) According to Anderson’s theorem, scattering leads to an averaging of the energy gap over the Fermi surface [69]. As revealed by our measurement of the superfluid density, scattering plays a substantial role for the superconductivity in Ti. Furthermore, in Ref. [34] it is shown that impurities can change the transition temperature of Ti by a factor of 2. Recent resistivity measurements indicate an anisotropy of the Debye frequency, which would lead to an anisotropy of the energy gap in the case of phononic coupling [70]. Depending on the amount of defect scattering (which we may have modified by polishing, since we only probe within a few hundred nm from the surface), the maximum energy gap on the Fermi surface has different values, and therefore the samples will vary in T_c . Furthermore, as mentioned in Sec. I, Ti exhibits several electronic bands crossing the Fermi energy, making Ti potentially a multiband and multigap superconductor. Depending on the strength of interband scattering, the potentially different energy gaps of different bands will average, leaving a single superconducting energy gap throughout the complete Fermi surface [71]. That we do not detect any signs of multiple energy gaps present in superconducting Ti therefore is consistent with the observed scattering rate that is much larger than the energy gap.

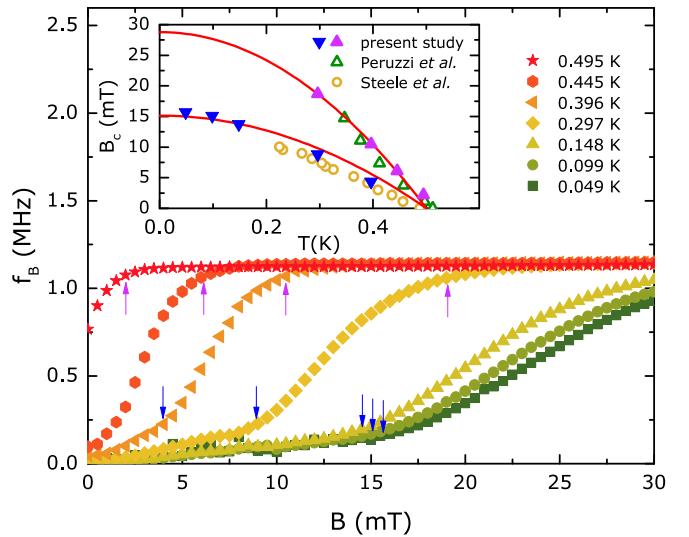


FIG. 7. Magnetic field dependence of the resonator bandwidth f_B measured at different temperatures up to T_c . The blue and purple arrows indicate the beginning and end of the superconducting transition. The resulting temperature dependence of the two field scales is plotted in the inset, together with the data reported by Steele *et al.* and Peruzzi *et al.* [33,35]. The red lines are fits according to Eq. (5).

D. Behavior in magnetic field

Titanium is a type I superconductor [72], i.e., any magnetic field is expelled from the interior of the sample until the external applied field reaches the value B_c . Figure 7 shows the magnetic field dependence of the measured resonator bandwidth f_B for different temperatures up to T_c . Interestingly the superconducting transition driven by magnetic field appears much broader than the one in zero field driven by temperature. Similarly, a broadening of the superconducting transition in Ti with increasing static external magnetic field has been reported in Ref. [34]. To quantify this effect, we read out the start and end of the superconducting transition, marked by blue and purple arrows, respectively, in Fig. 7. The resulting temperature dependence of these characteristic magnetic fields is shown in the inset of Fig. 7 as blue and purple triangles. In previous studies on the temperature dependence of the critical field of superconducting Ti with a similar T_c , rather diverse values for the critical fields have been reported [33,34]. Comparing our two field scales with those in literature we find good correspondence with both, which suggests that the broad transition of superconducting Ti is responsible for the large scattering reported in literature. The solid lines in Fig. 7 are fits to [67]

$$B_c(T) = B_c(0) \left(1 - \left(\frac{T}{T_c} \right)^2 \right). \quad (5)$$

The fits properly describe our experimental data and thus confirm the conventional parabolic temperature dependence that one expects for the critical magnetic field. Unfortunately, we cannot explicitly assign either of the two field scales to the conventional definition of B_c : microwave spectroscopy on type I superconductors previously found a similar effect for Pb that

was ascribed to surface superconductivity, but that observation was in a rather narrow field range compared to the present observation (and even narrower or absent for Sn) [53], and thus it is not clear to what extent this explanation can also be applied to the present case of Ti.

V. SUMMARY

We performed resonant microwave measurements on superconducting titanium using stripline resonators and determined the optical conductivity $\sigma(\omega, T)$ in frequency and temperature ranges 3–40 GHz and 40–600 mK. Qualitatively the frequency and temperature dependence of $\sigma(\omega, T)$ is in excellent agreement with the predictions of the Mattis-Bardeen theory. We can observe unique signatures of the energy gap 2Δ in the frequency and temperature dependence of σ_1 , and from the latter we can determine the temperature dependence of 2Δ , which is consistent with the BCS temperature dependence in the weak coupling limit with a ratio of $2\Delta/k_B T_c \approx 3.53$. Therefore we conclude that Ti is a BCS-like superconductor.

The temperature dependence of the superfluid density, obtained from the imaginary part of the optical conductivity, allows us to determine the absolute value of the scattering rate $\overline{\Gamma_{sf}}/2\pi = 418 \pm 43$ GHz, which compares well with the value determined from resistivity $\Gamma_\rho/2\pi = 490$ GHz. These scattering rates clearly indicate Ti being a superconductor in the dirty limit. From the absolute values of the superfluid density we determine the zero-temperature penetration depth $\overline{\lambda_0} = 238 \pm 9$ nm.

ACKNOWLEDGMENTS

We thank G. Untereiner for resonator and sample preparation, A. Löhle for support with the dc measurement, and D. M. Broun and N. R. Lee-Hone for fruitful discussions. M.T. thankfully acknowledges financial support by the Carl-Zeiss-Stiftung. We thankfully acknowledge financial support by the Deutsche Forschungsgemeinschaft (DFG).

-
- [1] D. N. Basov and T. Timusk, *Rev. Mod. Phys.* **77**, 721 (2005).
- [2] U. S. Pracht, E. Heintze, C. Clauss, D. Hafner, R. Bek, D. Werner, S. Gelhorn, M. Scheffler, M. Dressel, D. Sherman, B. Gorshunov, K. S. Ilin, D. Henrich, and M. Siegel, *IEEE Trans. THz Sci. Technol.* **3**, 269 (2013).
- [3] R. E. Glover and M. Tinkham, *Phys. Rev.* **108**, 243 (1957).
- [4] D. M. Ginsberg and M. Tinkham, *Phys. Rev.* **118**, 990 (1960).
- [5] M. Dressel, *Adv. Cond. Matter Phys.* **2013**, 104379 (2013).
- [6] J. Bardeen, L. N. Cooper, and J. R. Schrieffer, *Phys. Rev.* **108**, 1175 (1957).
- [7] W. N. Hardy, D. A. Bonn, D. C. Morgan, R. Liang, and K. Zhang, *Phys. Rev. Lett.* **70**, 3999 (1993).
- [8] F. Gao *et al.*, *Appl. Phys. Lett.* **63**, 2274 (1993).
- [9] D. A. Bonn *et al.*, *Phys. Rev. B* **47**, 11314 (1993).
- [10] A. Maeda, H. Kitano, and R. Inoue, *J. Phys.: Condens. Matter* **17**, R143 (2005).
- [11] A. Charnukha, *J. Phys.: Condens. Matter* **26**, 253203 (2014).
- [12] S. Tajima, *Rep. Prog. Phys.* **79**, 094001 (2016).
- [13] D. N. Basov, S. V. Dordevic, E. J. Singley, W. J. Padilla, K. Burch, J. E. Elenewski, L. H. Greene, J. Morris, and R. Schickling, *Rev. Sci. Instrum.* **74**, 4703 (2003).
- [14] R. Crane, N. P. Armitage, A. Johansson, G. Sambandamurthy, D. Shahar, and G. Grüner, *Phys. Rev. B* **75**, 184530 (2007).
- [15] N. H. Khah, G. V. S. Rao, M. Reedyk, H. Fujiwara, H. Kobayashi, T. Nakamura, K. Yakushi, and M. A. Tanatar, *Phys. Rev. B* **81**, 092508 (2010).
- [16] W. Liu, M. Kim, G. Sambandamurthy, and N. P. Armitage, *Phys. Rev. B* **84**, 024511 (2011).
- [17] K. Steinberg, M. Scheffler, and M. Dressel, *Rev. Sci. Instrum.* **83**, 024704 (2012).
- [18] E. F. C. Driessen, P. C. J. J. Coumou, R. R. Tromp, P. J. de Visser, and T. M. Klapwijk, *Phys. Rev. Lett.* **109**, 107003 (2012).
- [19] M. Scheffler, M. Thiemann, M. Beutel, U. S. Pracht, and M. Dressel, in *42nd International Conference on Infrared, Millimeter, and Terahertz Waves (IRMMW-THz)* (IEEE, Piscataway, NJ, 2017).
- [20] C. Pfeleiderer, *Rev. Mod. Phys.* **81**, 1551 (2009).
- [21] V. F. Gantmakher and V. T. Dolgoplov, *Phys. Usp.* **53**, 1 (2010).
- [22] U. S. Pracht, N. Bachar, L. Benfatto, G. Deutscher, E. Farber, M. Dressel, and M. Scheffler, *Phys. Rev. B* **93**, 100503(R) (2016).
- [23] K. Behnia, *Science* **355**, 26 (2017).
- [24] A. D. Caviglia, S. Gariglio, N. Reyren, D. Jaccard, T. Schneider, M. Gabay, S. Thiel, G. Hammerl, J. Mannhart, and J.-M. Triscone, *Nature (London)* **456**, 624 (2008).
- [25] R. J. Ormeno, A. Sibley, C. E. Gough, S. Sebastian, and I. R. Fisher, *Phys. Rev. Lett.* **88**, 047005 (2002).
- [26] R. J. Ormeno, M. A. Hein, T. L. Barraclough, A. Sibley, C. E. Gough, Z. Q. Mao, S. Nishizaki, and Y. Maeno, *Phys. Rev. B* **74**, 092504 (2006).
- [27] C. J. S. Truncik, W. A. Huttema, P. J. Turner, S. Özcan, N. C. Murphy, P. R. Carrière, E. Thewalt, K. J. Morse, A. J. Koenig, J. L. Sarrao, and D. M. Broun, *Nature Commun.* **4**, 2477 (2013).
- [28] M. Scheffler, M. M. Felger, M. Thiemann, D. Hafner, K. Schlegel, M. Dressel, K. S. Ilin, M. Siegel, S. Seiro, C. Geibel, and F. Steglich, *Acta IMEKO* **4**, 47 (2015).
- [29] Y. Wiemann, J. Simmendinger, C. Clauss, L. Bogani, D. Bothner, D. Koelle, R. Kleiner, M. Dressel, and M. Scheffler, *Appl. Phys. Lett.* **106**, 193505 (2015).
- [30] M. Li *et al.*, *New J. Phys.* **18**, 082001 (2016).
- [31] J. G. Daunt and C. V. Heer, *Phys. Rev.* **76**, 715 (1949).
- [32] T. S. Smith and J. G. Daunt, *Phys. Rev.* **88**, 1172 (1952).
- [33] M. C. Steele and R. A. Hein, *Phys. Rev.* **92**, 243 (1953).
- [34] A. Peruzzi, E. Gottardi, I. Peroni, G. Ponti, and G. Ventura, *Nucl. Phys. B* **78**, 576 (1999).
- [35] A. Peruzzi, E. Gottardi, and I. Peroni, G. Ventura, and F. Pavese, *Metrologia* **37**, 229 (2000).
- [36] W. Meissner, *Z. Phys* **60**, 181 (1930).
- [37] D. Shoenberg, *Proc. Camb. Phil. Soc.* **36**, 84 (1940).
- [38] G. N. Kamm and J. R. Anderson, *Low Temp. Phys.* LT-13 **4**, 114 (1974).
- [39] R. M. Welch and E. H. Hygh, *Phys. Rev. B* **9**, 1993 (1974).

- [40] M. Ruby, B. W. Heinrich, J. I. Pascual, and K. J. Franke, *Phys. Rev. Lett.* **114**, 157001 (2015).
- [41] H. B. Heersche, P. Jarillo-Herrero, J. B. Oostinga, L. M. K. Vandersypen, and A. F. Morpurgo, *Nature (London)* **446**, 56 (2007).
- [42] B. Sacépé, J. B. Oostinga, J. Li, A. Ubal dini, N. J. G. Couto, E. Giannini, and A. F. Morpurgo, *Nature Commun.* **2**, 575 (2011).
- [43] M. R. Vissers, J. Gao, M. Sandberg, S. M. Duff, D. S. Wisbey, K. D. Irwin, and D. P. Pappas, *Appl. Phys. Lett.* **102**, 232603 (2013).
- [44] D. C. Mattis and J. Bardeen, *Phys. Rev.* **111**, 412 (1958).
- [45] M. S. DiIorio, A. C. Anderson, and B.-Y. Tsaur, *Phys. Rev. B* **38**, 7019 (1988).
- [46] M. Scheffler, C. Fella, and M. Dressel, *J. Phys.: Conf. Ser.* **400**, 052031 (2012).
- [47] M. Scheffler, K. Schlegel, C. Clauss, D. Hafner, C. Fella, M. Dressel, M. Jourdan, J. Sichelschmidt, C. Krellner, C. Geibel, and F. Steglich, *Phys. Status Solidi B* **250**, 439 (2013).
- [48] D. Hafner, M. Dressel, and M. Scheffler, *Rev. Sci. Instr.* **85**, 014702 (2014).
- [49] O. Klein, S. Donovan, M. Dressel, and G. Grüner, *Int. J. Infrared Millimeter Waves* **14**, 2423 (1993).
- [50] M. Dressel and G. Grüner, *Electrodynamics of Solids* (Cambridge University Press, Cambridge, 2002).
- [51] H. A. Wheeler, *IEEE Trans. Microwave Theor. Techniques* **26**, 866 (1978).
- [52] J. Krupka *et al.*, *Meas. Sci. Technol.* **10**, 387 (1999).
- [53] N. G. Ebensperger, M. Thiemann, and M. Dressel, and M. Scheffler, *Supercond. Sci. Technol.* **29**, 115004 (2016).
- [54] The sample was bought from Goodfellow GmbH.
- [55] M. A. Ordal, R. J. Bell, R. W. Alexander, and L. L. Long, and M. R. Querry, *Appl. Opt.* **24**, 4493 (1985).
- [56] C. Attanasio, L. Maritato, and R. Vaglio, *Phys. Rev. B* **43**, 6128 (1991).
- [57] J. M. Pierce, *J. Appl. Phys.* **44**, 1342 (1973).
- [58] K. Holczer, O. Klein, and G. Grüner, *Solid State Commun.* **78**, 875 (1991).
- [59] F. Marsiglio *et al.*, *Phys. Rev. B* **50**, 7203(R) (1994).
- [60] O. Klein *et al.*, *Phys. Rev. B* **50**, 6307 (1994).
- [61] B. B. Jin, T. Dahm, A. I. Gubin, E.-M. Choi, H. J. Kim, S.-I. Lee, W. N. Kang, and N. Klein, *Phys. Rev. Lett.* **91**, 127006 (2003).
- [62] K. Steinberg, M. Scheffler, and M. Dressel, *Phys. Rev. B* **77**, 214517 (2008).
- [63] A. V. Pronin, M. Dressel, A. Pimenov, A. Loidl, I. V. Roshchin, and L. H. Greene, *Phys. Rev. B* **57**, 14416 (1998).
- [64] X. Xi, J. Hwang, C. Martin, D. B. Tanner, and G. L. Carr, *Phys. Rev. Lett.* **105**, 257006 (2010).
- [65] U. S. Pracht, M. Scheffler, M. Dressel, D. F. Kalok, C. Strunk, and T. I. Baturina, *Phys. Rev. B* **86**, 184503 (2012).
- [66] W. Zimmermann, E. Brandt, M. Bauer, E. Seider, and L. Genzel, *Physica C: Supercond.* **183**, 99 (1991).
- [67] M. Tinkham, *Introduction to Superconductivity*, 2nd ed. (McGraw-Hill, New York, 1996).
- [68] S. B. Nam, *Phys. Rev.* **156**, 470 (1967).
- [69] P. W. Anderson, *J. Phys. Chem. Solids* **11**, 26 (1959).
- [70] L. S. S. Chandra, R. Mondal, A. Thamizhavel, S. K. Dhar, and S. B. Roy, *Physica B* **521**, 175 (2017).
- [71] M. Thiemann, M. H. Beutel, M. Dressel, N. R. Lee-Hone, D. M. Broun, E. Fillis-Tsirakis, H. Boschker, J. Mannhart, and M. Scheffler, *Phys. Rev. Lett.* **120**, 237002 (2018).
- [72] Whether a superconductor is type I or type II is defined by the ratio $\kappa = \lambda/\xi_{GL}$ where ξ_{GL} is the Ginzburg-Landau coherence length [67]. In the dirty limit $\xi_{GL} = 0.885\sqrt{\xi_{BCS}l}$ with $\xi_{BCS} = \hbar v_F/(\pi \Delta_0)$ the BCS coherence length, $l = v_F/\Gamma$ the mean free path, v_F the Fermi velocity. As Ti is a conventional elemental metal, one can expect $v_F \approx 10^6$ m/s. Taking our obtained scattering rate $\Gamma = 418$ GHz and zero-temperature energy gap $\Delta_0 = 75$ μ eV, we obtain an estimate for the coherence length of $\xi_{GL} \approx 2$ μ m. With $\lambda_0 = 238$ nm this results in $\kappa \approx 0.1 \ll 1/\sqrt{2}$ placing our samples deep in the regime of type I superconductors.